PARTICLE-FLUID HYBRID SIMULATIONS APPLIED TO BEAM-PLASMA AND RING-PLASMA INSTABILITIES

by

Jae Koo Lee and C. K. Birdsall

Memorandum No. UCB/ERL M79/15

26 February 1979

ELECTRONICS RESEARCH LABORATORY

College of Engineering
University of California, Berkeley
94720

TABLE OF CONTENTS

ABSTRACT

A particle simulation usually suffers from a high level of unphysical noise unless a large number of particles are used. To improve this situation, a hybrid scheme is used replacing the general particle mover by a linearized fluid mover for those species of ions and electrons which do not undergo large amplitude perturbations and keeping the fully nonlinear particle mover for those species which experience more violent changes. The structure of these hybrid codes (electrostatic and electromagnetic) is shown with two applications, which produce excellent agreement with linear and nonlinear theories plus substantial reduction in the noise level and the computing cost. The use of the linearized fluid equations is justified through monitoring v_{fluid}/v_{wave}, to guarantee that it stays small.

I. INTRODUCTION

Beam-plasma-type instabilities which are simulated using particle codes require a very large number of simulation particles for the plasma part, which is usually 100 to 1000 times denser than the beam part, in order that the noise from the plasma particles does not obscure the instability. An example of this difficulty was observed in the simulation of the velocity space ring-plasma (flute-like) instability, which was due to the interactions of energetic beam ions (a ring in velocity space) with cooler Maxwellian plasma ions as carried out through a particle code by Birdsall et al. [1]. In order to reduce the plasma noise, Langdon [2] suggested the construction of a hybrid code using particles for simulation of the beam and a linearized fluid for the plasma. The linearization needs to be monitored but it is generally justifiable since the plasma component stays linear in most weak beam-strong plasma interactions [3]. Our particle-fluid hybrid scheme will be discussed in detail. Applications of two hybrid codes, electrostatic and electromagnetic, will be given to the study of linear and nonlinear evolution of the magnetized ring-plasma instability and the usual beam-plasma instability. Note that the use of a hybrid for a beam-plasma-type instability not only has the merit of eliminating the noise from the plasma particles but also reduces computing cost drastically (one fluid equation integration in place of many plasma particle integrations) with only little effect on the physical properties.

The hybrid simulation of an unmagnetized beam-plasma instability yields results (linear and nonlinear) almost identical to those using a wholly particle code. However, for the ring-plasma instability the difference between hybrid and particle simulations is appreciable; the hybrid code provides remarkable verification of the linear Vlasov theory compared with the particle code results. This excellent agreement extends to a wide range of parameters whether electrostatic or electromagnetic. Hybrid simulations also provide extensive information about nonlinear evolution of this instability such as collisionless beam spreading, average slowing down, and saturation level, which agree well with analytic explanations.

In Sec. II, the structure of these hybrid codes is shown. In Sec. III, the application of these codes to the ring-plasma instability is given, including comparison to theoretical analyses and wholly particle simulation. In Sec. IV, application to the unmagnetized beam-plasma instability is given with some new results (theory and simulation) on saturation effects. Section V is the conclusion.

II. STRUCTURE OF HYBRID CODES

(1) Electrostatic Version

The electrostatic hybrid code consists of the particle code (ES1, electrostatic 1d) and the fluid code (EFL, Eulerian fluid, linearized, 1d). The particle code (written by Langdon) is used for the beam particles, as the beam can exhibit highly nonlinear behavior. The fluid part uses the linearized Eulerian fluid equations which are adequate for simulating the plasma component which experiences only small-amplitude fluctuations.

The structure of ES1 is well-known [4]. In the following we describe a one dimensional version of EFL.

The equations for a collisionlesss charged fluid in Eulerian form [5] are the equation of continuity

$$\frac{\partial \rho}{\partial t} + \nabla \cdot (\rho \underline{v}) = 0 \tag{1}$$

the equation of motion

$$\frac{\partial \underline{v}}{\partial t} + (\underline{v} \cdot \nabla)\, \underline{v} = \frac{q}{m} (\underline{E} + \underline{v} \times \underline{B}) - \frac{\nabla p}{nm} \tag{2}$$

the equation of state (adiabatic)

$$\frac{p}{\rho^{\gamma}} = \text{constant} \tag{3}$$

$$p_0 = n_0 \kappa T \tag{4}$$

and the field equations

$$\nabla \cdot \underline{E} = \rho/\varepsilon_0 \tag{5}$$

$$\underline{E} = -\nabla\phi \tag{6}$$

where $\rho = nq$ is the charge density of a fluid element and γ is the ratio of specific heats; the rest of the symbols are standard.

Equations (1)-(4) are to be written for as many fluids as are being used, each with its own $\underline{v}$, p, ρ and γ.

This set of fluid equations is only one of several sets that might be used. Other sets can be made, for example, by keeping different numbers of moments of the kinetic equation. Equation (1) comes from taking the zero-th order moment (fluid number density $\sim \int f\, d\underline{v}$) and Eq. (2) comes from the first order moment (fluid momentum $\sim \int m\underline{v}\, f\, d\underline{v}$). Equation (3) closes the set. Keeping the next moment (which is fluid energy $\sim \int nm\underline{v}^2\, f\, d\underline{v}$) would have produced the heat-flow equation. This was not done here, implying that there is no heat flow from one element of the fluid to another. Had the third moment been retained, then it would have been necessary to assign an (internal) energy density to each fluid element (grid cell), and provide an equation for the evolution of the energy density.

Prior work with charged and magnetized fluids is both extensive and sophisticated. The ideas of mixing fluids and particles and where to place closure are far less extensive and developed. Two challenging codes and initial results are those of Marder [6] and Anderson [7].

The linearization of Eqs. (1) & (2) for a nondrifting plasma (which drops the potentially bothersome advective term $\underline{v} \cdot \nabla\underline{v}$) in an applied magnetic field $\underline{B}_0$ are

$$\frac{\partial \underline{v}_1}{\partial t} = \frac{q}{m} (\underline{E}_1 + \underline{v}_1 \times \underline{B}_0) - \gamma \frac{v_t^2}{\rho_0} \nabla \rho_1 \tag{7}$$

$$\frac{\partial \rho_1}{\partial t} = - \rho_0 \nabla \cdot \underline{v}_1 \tag{8}$$

where

$$\rho_0 = n_0 q \quad , \quad \rho_1 = n_1 q \quad , \quad v_t^2 = \kappa \frac{T}{m} \quad \text{and} \quad \gamma = \frac{f+2}{f}$$

where f is the number of the degrees of freedom ($\gamma = 3$ for one spatial dimension).

For the numerical model of the fluid, the first-order quantities (subscript 1 now dropped) $\underline{v}$, ρ and $\underline{E}$ are grid quantities, which may be centered spatially and temporally, as shown in Fig. 1. In finite-differencing, Eqs. (7) and (8) become in one dimensional form

$$\frac{v_{j+\frac{1}{2}}^{n+\frac{1}{2}} - v_{j+\frac{1}{2}}^{n-\frac{1}{2}}}{\Delta t} = \frac{q}{m} \left[E_{j+\frac{1}{2}}^{n} + \left(\frac{v_{j+\frac{1}{2}}^{n+\frac{1}{2}} + v_{j+\frac{1}{2}}^{n-\frac{1}{2}}}{2} \times B_0 \right) \right] - \frac{\gamma v_t^2}{\rho_0} \left(\frac{\rho_{j+1}^{n} - \rho_j^{n}}{\Delta x} \right) \tag{7}'$$

$$\frac{\rho_j^{n+1} - \rho_j^{n}}{\Delta t} = - \rho_0 \left(\frac{v_{j+\frac{1}{2}}^{n+\frac{1}{2}} - v_{j-\frac{1}{2}}^{n+\frac{1}{2}}}{\Delta x} \right) \tag{8}'$$

Equations (7)' and (8)' form a leap-frog pair, which are second-order accurate in the time integration.

The fluid dispersion relation and consistent excitations are readily obtained. In the absence of $\underline{B}_0$ field, the linearized equations are

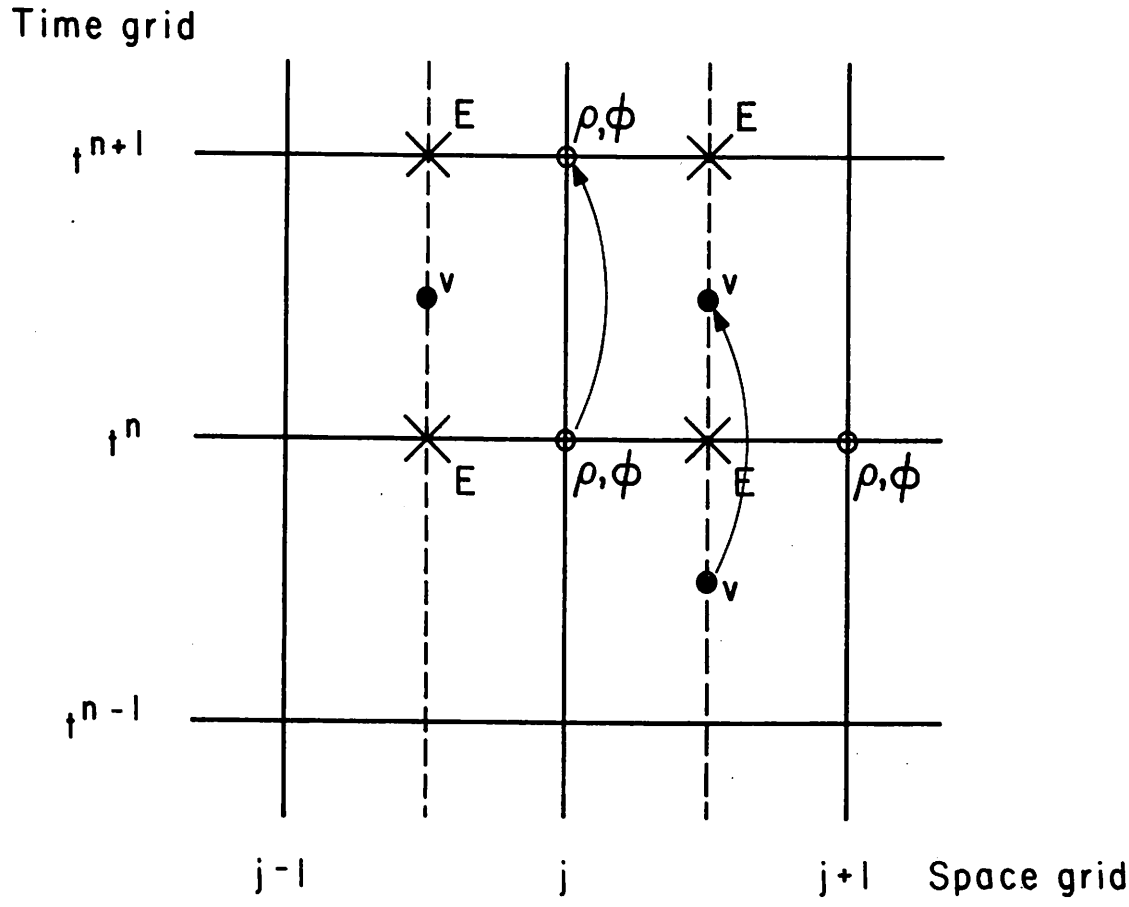

Fig. 1 Time and space centered leap-frog grids. $E^n_{j+\frac{1}{2}}$ is calculated using ϕ^n_j and ϕ^n_{j+1} for the two-point scheme. $v^{n-\frac{1}{2}}_{j+\frac{1}{2}}$ is advanced to $v^{n+\frac{1}{2}}_{j+\frac{1}{2}}$ using $E^n_{j+\frac{1}{2}}$, ρ^n_j and ρ^n_{j+1}. Then, ρ^n_j is advanced to ρ^{n+1}_j using $v^{n+\frac{1}{2}}_{j+\frac{1}{2}}$ and $v^{n+\frac{1}{2}}_{j-\frac{1}{2}}$.

$$\left.\begin{aligned} \frac{\partial v_1}{\partial t} &= \frac{q}{m} E_1 - \frac{\gamma v_t^2}{\rho_0} \frac{\partial \rho_1}{\partial x} \\ \frac{\partial \rho_1}{\partial t} &= -\rho_0 \frac{\partial v_1}{\partial x} \\ \frac{\partial E_1}{\partial x} &= \frac{\rho_1}{\varepsilon_0} \end{aligned}\right\} \tag{9}$$

Assuming traveling wave solutions of the form

$$\left.\begin{aligned} v_1(x,t) &= V \sin (kx - \omega t) \\ E_1(x,t) &= \xi \cos (kx - \omega t) \\ \rho_1(x,t) &= R \sin (kx - \omega t) \end{aligned}\right\} \tag{10}$$

the above set produces the familiar dispersion relation of Bohm and Gross

$$\omega^2 = \omega_p^2 + \gamma k^2 v_t^2 \ . \tag{11}$$

For initial velocity modulation as

$$v_1(x,0) = V \sin kx \tag{12}$$

the corresponding density modulation is

$$\rho_1(x,0) = \frac{k}{\omega} \rho_0 V \sin kx \tag{13}$$

where k and ω are related as in Eq. (11).

The effect of the spatial grid is as follows. Assume that all variables behave as $\exp(-i\omega t)$ and let $\Delta t \to 0$. Let the four spatial

derivatives be replaced by ik_1 , ik_2 , ik_3 and ik_4 , all to be obtained from finite differences. Then Eqs. (9) become

$$\left.\begin{aligned} -i\omega v_1 &= -\frac{q}{m}\, i\, k_1\phi - \frac{\gamma v_t^2}{\rho_0}\, ik_2\, \rho_1 \\ -i\omega\rho_1 &= -\rho_0\, ik_3\, v_1 \\ -k_4^2\phi &= -\frac{\rho_1}{\varepsilon_0} \end{aligned}\right\} \qquad (14)$$

The new dispersion relation is

$$\omega^2 = \omega_p^2 \frac{k_1 k_3}{k_4^2} + \gamma v_t^2\, k_2 k_3 \qquad (15)$$

The four k's are now calculated. Since $\underline{E} = -\nabla\phi$ and $\underline{E}$ is defined and wanted between grid points, we use the two-point scheme

$$E_{j+\frac{1}{2}} = \frac{\phi_{j+1} - \phi_j}{-\Delta x}$$

Assuming that all variables may be expanded in a finite Fourier series, as

$$\phi_j \equiv \phi(x_j) = \frac{1}{L} \sum_{j=0}^{NG-1} \phi(k)\, \exp\,(ijk\,\Delta x)\ ,$$

where NG is the number of spatial grids, we obtain

$$k_1 = k\ \mathrm{dif}\ (\tfrac{1}{2}\, k\, \Delta x)$$

where

$$\text{dif}\ (y) \equiv \frac{\sin y}{y}$$

Likewise

$$k_2 = k_3 = k_4 = k\ \text{dif}\ (\tfrac{1}{2}k\Delta x)$$

Thus, Eq. (15) becomes

$$\omega^2 = \omega_p^2 + \gamma v_t^2\, k^2\, \text{dif}^2\ (\tfrac{1}{2}k\Delta x) \tag{16}$$

Similarly, for $\Delta t \neq 0$, we obtain

$$\omega = \frac{2}{\Delta t}\ \sin^{-1}\left\{\left(\pm\frac{\Delta t}{2}\right)\left[\omega_p^2 + \gamma v_t^2 k^2\ \text{dif}^2\left(\frac{k\Delta x}{2}\right)\right]^{\frac{1}{2}}\right\} \tag{16}'$$

As an alternative to Eq. (16), let the $\underline{E}$ field be given at the grid points as for the particles in ES1, so in Eq. (9)', the centered $E_{j+\frac{1}{2}}$ is

$$E^n_{j+\frac{1}{2}} = \frac{1}{2}\,(E^n_{j+1} + E^n_j)$$

$$= \frac{1}{2}\left[\frac{\phi_{j+1} - \phi_{j-1}}{(-2\Delta x)} + \frac{\phi_{j+2} - \phi_j}{(-2\Delta x)}\right]$$

Then the dispersion relation becomes

$$\omega^2 = \omega^2\ [\cos^2\ (\tfrac{1}{2}k\Delta x)] + \gamma v_t^2\ \text{dif}^2\ (\tfrac{1}{2}k\Delta x) \tag{17}$$

which is more dispersive than Eq. (16) and will not be used further.

As a third alternative to Eq. (16), if we use a non-space-centered $\underline{E}$, such as that in ES1,

$$E_j = \frac{\phi_{j+1} - \phi_{j-1}}{-2\Delta x} ,$$

then ω^2 is complex, with growing and decaying roots and, hence, no good.

Simulation was done using this fluid code (EFL). It was tried for thermal plasma oscillations with various values of $\lambda_D/\Delta x$ in the absence of uniform $\underline{B}_0$ and also in the presence of $\underline{B}_0$ (the latter is not shown in the following).

Using the fluid alone, all modes were initiated randomly and showed clear plasma oscillations with almost no noise (and, of course, with no Landau damping). The simulation frequencies fit the dispersion relations Eqs. (16,17) very well ($\lesssim 3\%$) as shown in Fig. 2. The same results are plotted versus $k\lambda_D$ out to about 0.4, the usable range of the linearized fluid equations in Fig. 3.

Our hybrid scheme [8] combines EFL with ES1. Total energy variation is used as a check on the accuracy of the scheme. The largest change in total energy observed in most of our electrostatic hybrid simulations, for about 5000 time steps, was about 1%, which is generally of negligible importance.

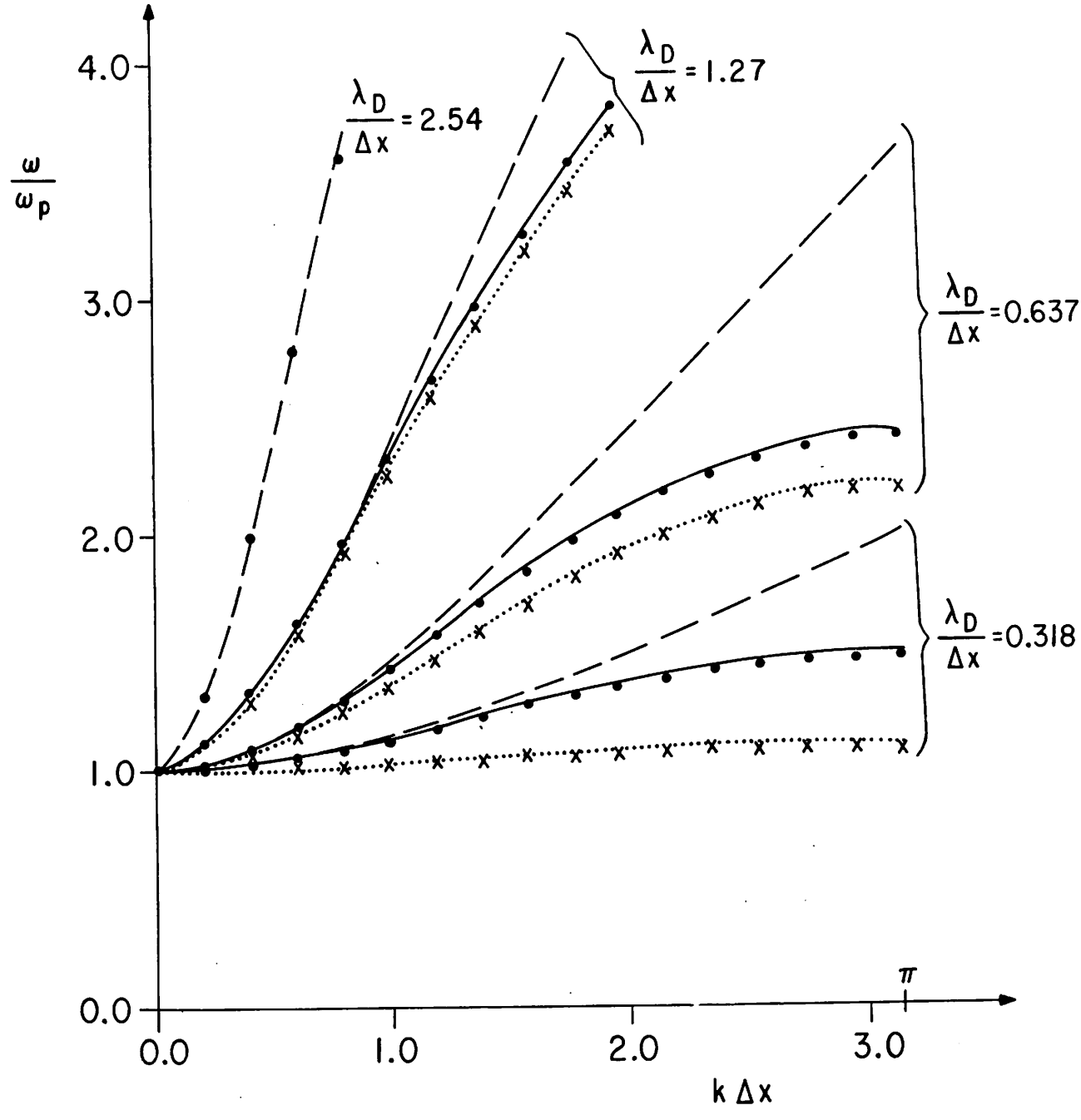

Fig. 2 Dispersion curves (ω vs $k\Delta x$) for fluid-plasma oscillation with no magnetic field. The dashed lines are the Bohm-Gross dispersions. The solid lines are the finite difference theoretical dispersions using the 2-point scheme. The dotted lines are the finite difference theoretical dispersions using the 4-point scheme. The simulation results for both schemes are indicated as points and crosses, respectively. Use of smaller $\lambda_D/\Delta x$ produces $\omega < \omega_p$ for the 4-point scheme (not shown).

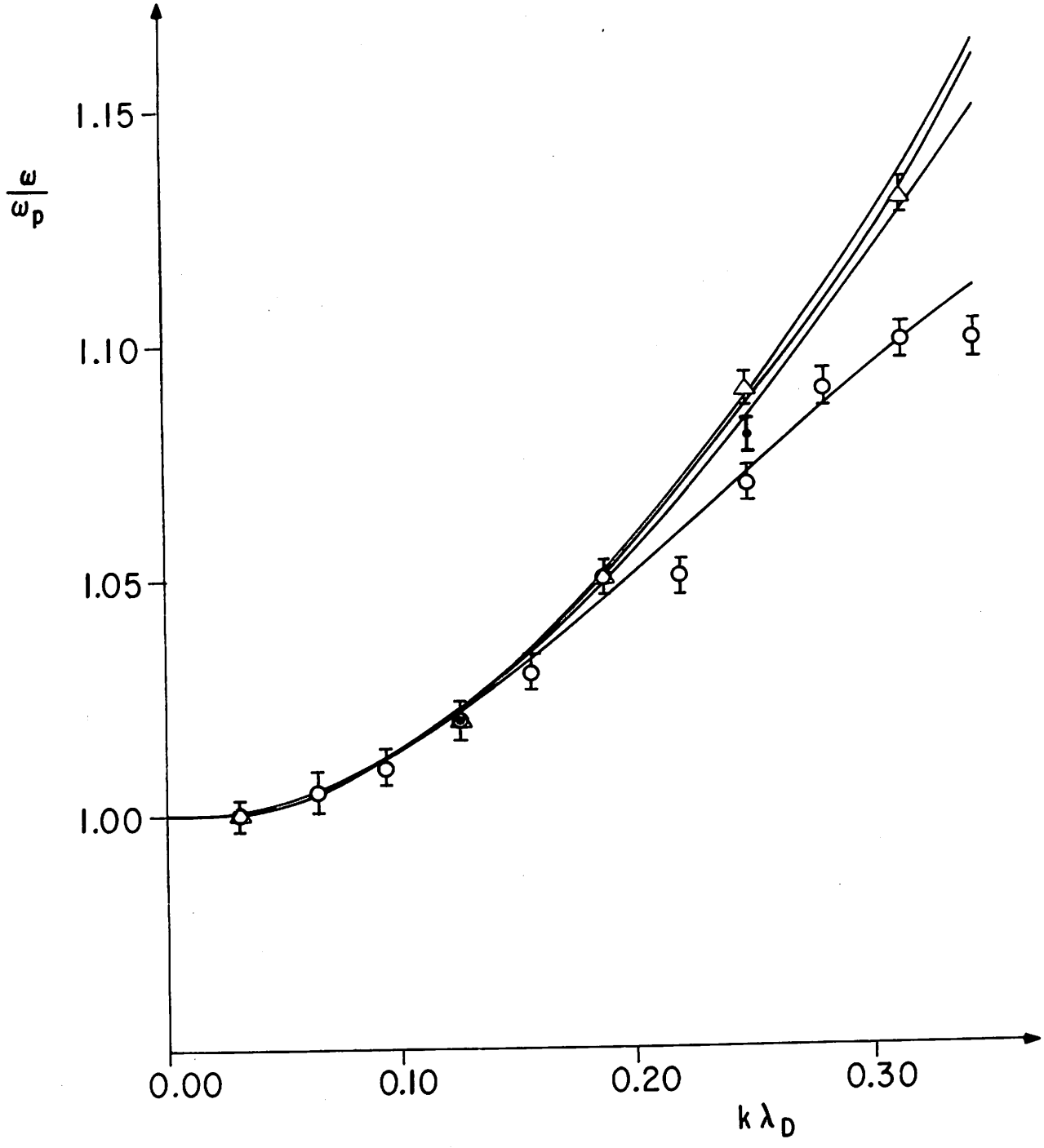

Fig. 3 Expanded dispersion curves (ω vs $k\lambda_D$) using the 2-point scheme. The top curve is the Bohm-Gross dispersion. The next curve is the 2-point theory for $\lambda_D/\Delta x = 0.637$; the next curve is for $\lambda_D/\Delta x = 0.318$; the last curve is for $\lambda_D/\Delta x = 0.159$. The simulation results are indicated as • , Δ , O , with error bars, in the same order.

(2) Electromagnetic Version

In the electromagnetic hybrid code we use the one dimensional electromagnetic code EM1 [9], and use a modified (so as to be electromagnetic) EFL for the dense plasma part.

As shown in Fig. 4, the additional quantities kept in this linearly polarized electromagnetic hybrid simulation are the radiation fields B_z and E_y and current J_y both by ring and plasma parts. Except for these, the scheme is almost identical to that of the electrostatic hybrid version as Fig. 5 is compared with Fig. 1.

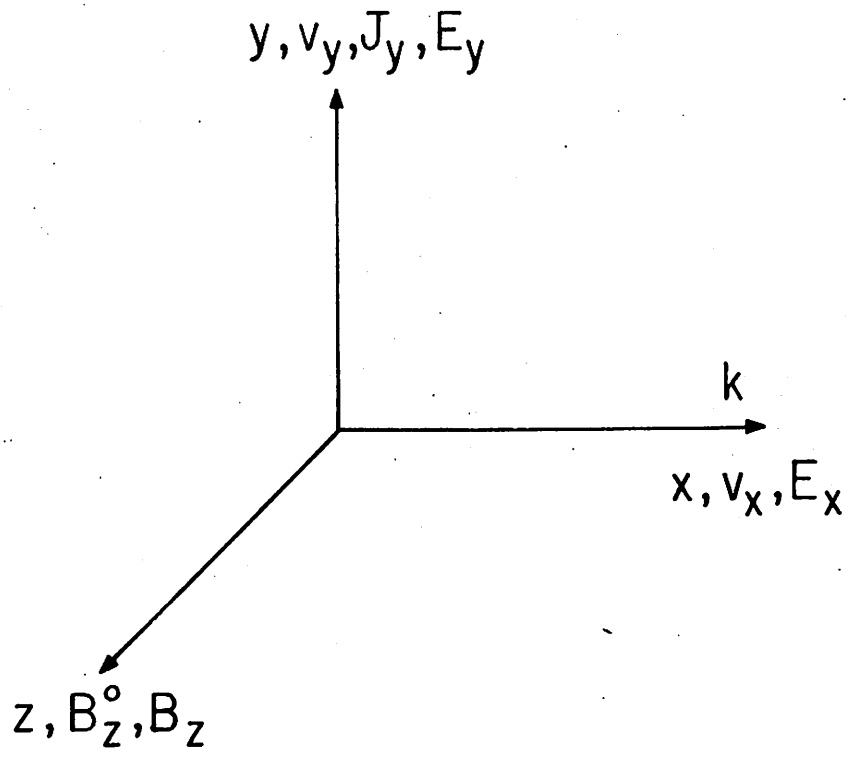

Fig. 4 The coordinates and the quantities used in our electromagnetic hybrid simulation. B_z^o is the applied uniform magnetic field, B_z and E_y are the induced radiation fields, and J_y is the induced transverse current.

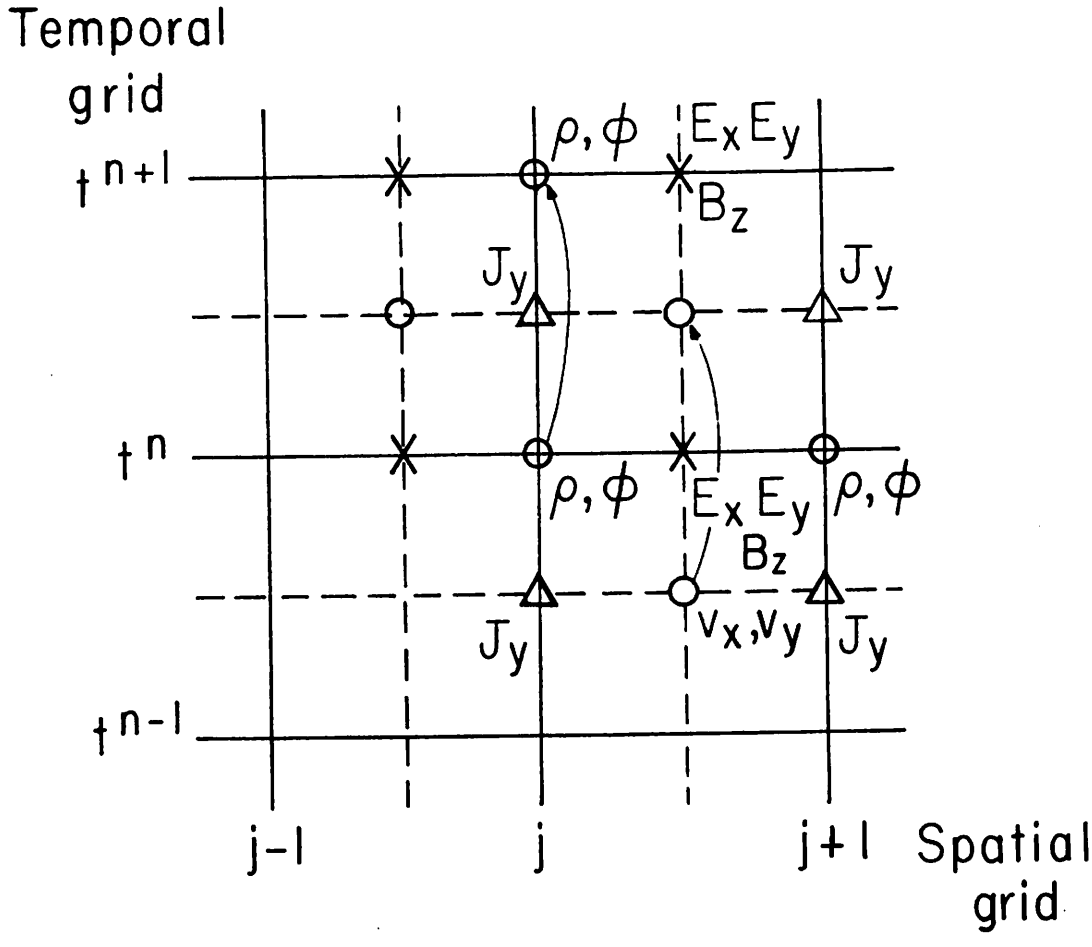

Fig. 5 The electromagnetic leap-frog scheme is similar to that of the electrostatic case (Fig. 1).

III. APPLICATION TO RING-PLASMA INSTABILITY

(1) General View

A neutral beam injected perpendicular to a magnetic field $\underline{B}_o$ into a target plasma becomes ionized and forms an energetic charged ring in the velocity-space perpendicular to $\underline{B}_o$. The interaction of this beam (now a ring) with a Maxwellian target plasma drives a flute-like ($k_\parallel = 0$) velocity-space instability. Recent laboratory experiments (Seiler et al. [10], Yamada et al. [11], and Böhmer [12] as as well as theoretical studies (Tataronis and Crawford [13], and Mynick et al. [14]) confirm this instability.

An early simulation for this instability was that of Birdsall and Maron [1] using a particle code. Their simulations had large noise due to the particles in the dense plasma component which almost obscured the instability itself, thus providing only a qualitative verification of the instability.

The hybrid codes described in the previous section have been used to study the ring-plasma instability. The complex frequencies of the hybrid simulations agree remarkably well with the linear Vlasov theory within a few percent both for electrostatic and for electromagnetic cases (for the widely varying electromagnetic effects).

In addition to the small amplitude behavior, hybrid simulations provide useful information on some nonlinear phenomena. The nonlinear evolution observed in simulations shows appreciable average slowing and broadening of the ring in $v_\perp$ space in a short time, on the order of an ion cyclotron period, at about the time the growing field

energy reaches its first peak value. The slowing and spreading are not due to collisions. Considerable structure has been observed in the velocity-space $v_\perp$ perpendicular to the magnetic field as predicted analytically. As nonlinear effects increase, the wave growth slows and reaches saturation. For most of ring to plasma density ratios, the saturation mechanism was found to be by trapping.

Details of these linear and nonlinear observation and checks with theoretical analyses as well as the comparison with the particle simulation results [1] are discussed elsewhere (Lee and Birdsall [15]).

Compared to the pure particle code [1], these hybrid codes [8] have much less noise because there is no noise from the denser Maxwellian plasma, and they require much less computing time while keeping the necessary number of particles to describe the physics properly. For cold plasma simulation, only a small number of particles is generally used. For a warm plasma, modelling with particles requires a larger number of particles to fill the 2v velocity space and 1d coordinate space; even then, the noise level, dependent on $1/\sqrt{N}$, may not be small. For the hybrid case cited here, we used 256 "particles" for the core with no noise (like $N \to \infty$).

(2) Justification of Linearized Fluid

The linearity assumption is good only when perturbed fluid plasma velocities v_1 remain small compared to the wave phase velocity ω/k. This is so because from the linearized continuity equation

$$\frac{\rho_1}{\rho_o} = \frac{v_1}{\omega/k - v_1} = \frac{v_1}{\omega/k}\left\{1 + \frac{v_1}{\omega/k} + \mathcal{O}\left[\left(\frac{v_1}{\omega/k}\right)^2\right]\right\} . \qquad (18)$$

We found that the linearization was satisfied except for the strong-beam regime at saturation. In order to check whether $v_1 \ll \omega/k$, kv_1/ω was continually monitored, as shown in Fig. 6. In Fig. 6, the maximum perturbed plasma velocity is seen to be not negligibly small only at large beam strength, i.e., at $R = 1$ (where R is the ratio of beam to plasma density) near and after the saturation. In order to allow larger nonlinearity in the fluid plasma, changing to a new model (e.g., using a Lagrangian fluid) is recommended.

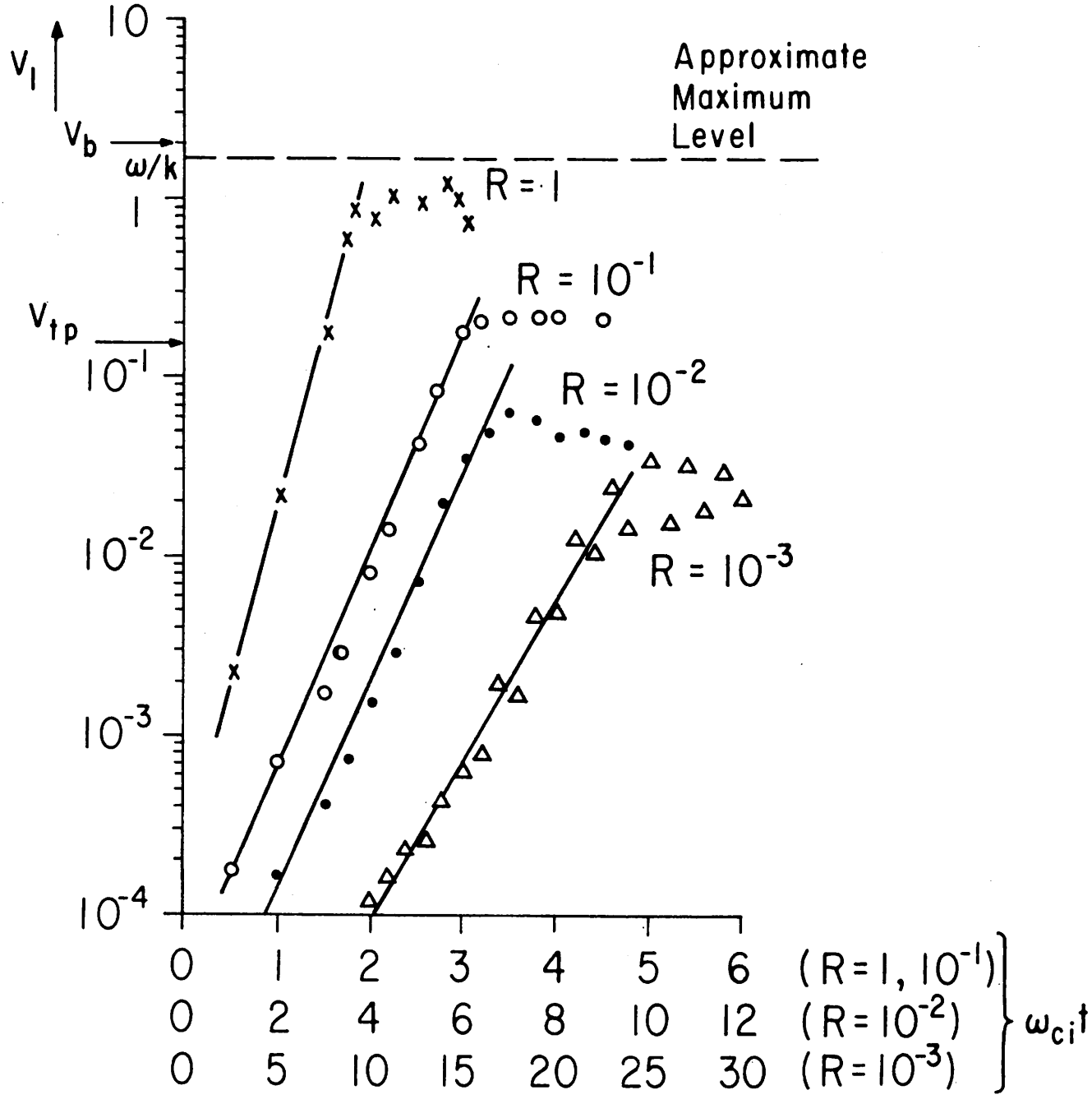

Fig. 6 The time evolution of the maximum perturbed plasma fluid velocities v_1 for $R = 1$, 10^{-1}, 10^{-2}, and 10^{-3}, obtained from electrostatic hybrid simulations of Ref. [14]. Note that the linearity assumption does not hold near the saturation time for strong beams where the wave phase velocity (ω/k) is only about 1.6 above the perturbed fluid velocities. Here, v_b and v_{tp} indicate the initial velocity of the beam and the plasma respectively, and ω_{ci} is the ion cyclotron frequency.

IV. APPLICATION TO BEAM-PLASMA INSTABILITY

(1) General View

The familiar beam-plasma instability in the absence of magnetic fields is readily simulated using the hybrid code. The linearized plasma like that of O'Neil et al. [3] is noiseless, allowing very low level effects to be followed. We have used this code in this manner, and also to obtain saturation behavior where the plasma remains linear, but the much weaker beam becomes highly nonlinear. In the latter, we found that the peak amplitude (saturation) of electrostatic field energy, for essentially single mode excitation fell off very rapidly for k away from that for maximum linear growth, γ_{max}, more rapidly than did γ/γ_{max}. This is somewhat new but predicted by single mode trapping theory and verified using both particle code ES1 and the hybrid code ES1 + EFL.

(2) Off-peak Saturation Effects

The single wave trapping theory of Drummond et al. [16] provides a rough estimation of the saturation level of the electrostatic field energy ESE relative to the initial beam kinetic energy $KE_{o,b}$ for a weak cold beam-cold plasma instability (with no magnetic field).

The saturation level is defined as

$$\eta \equiv \frac{\overline{ESE}}{KE_{o,b}} \equiv \frac{\frac{1}{4}\varepsilon_o E^2_{\text{first peak}}}{\frac{1}{2}m_b n_b v_b^2} \tag{19}$$

From Ref. [16], it is shown that

$$\eta \approx \frac{2\Delta v}{v_b} \tag{20}$$

where Δv is the difference between beam and phase velocities. If the theoretically most unstable mode (i.e., the fastest growing mode $\gamma = \gamma_{max}$ when the spectrum is dense and continuous, roughly at $kv_b/\omega_{pp} \approx 1.0$) is allowed to grow, then the wave saturation is dominated by this fastest growing mode. That is, a single wave structure exists at least up to the first peak or saturation. In this single wave $\gamma = \gamma_{max}$ case, Eq. (20) takes the more useful form, as in Ref. [16]

$$\eta = \left(\frac{R}{2}\right)^{1/3} \tag{21}$$

where

$$R \equiv \frac{n_b}{n_p} = \left(\frac{\omega_{pb}}{\omega_{pp}}\right)^2$$

n_b , n_p are beam and plasma densities, respectively, and ω_{pb} , ω_{pp} are plasma frequencies of the beam and the plasma, respectively.

However, if for some reasons the physical system does not allow the excitation of the most unstable mode, allowing for only a single wave at $kv_b/\omega_{pp} \neq 1.0$, where $\gamma \equiv \gamma_{max}$, then the estimation formula, Eq. (21), should be modified because in deriving Eq. (21), it was assumed that the phase was that of the most unstable mode. This study was initially

motivated by a computer simulation using $R = 0.001$ and only a single wave at $kv_b/\omega_{pp} = 0.8$ with $\gamma < \gamma_{max}$. We were surprised to find $\eta = 0.01$, which is much less than $\eta = 0.079$ predicted by Eq. (21).

First we will estimate η for a wide range of kv_b/ω_{pp}, using the single wave nonlinear trapping argument of Ref. [16]; that is, Eq. (20) will still be used to relate η and Δv. (This relation needs modification when the plasma is not cold.) Next we will then compare the estimate with simulation results both by a particle code (ES1) and by the hybrid (ES1 + EFL) code.

In simulations we fixed the beam strength at $R = 0.001$, and observed the saturation level η and the maximum growth rate γ/ω_{pp} by changing the parameter kv_b/ω_{pp}. We varied v_b; changing any other parameter (k or ω_{pp}) yield similar results in those cases that were checked.

(a) Estimation of Saturation Level

The dielectric function of the cold beam-cold plasma system is written as

$$\varepsilon(k,\omega) = 1 - \frac{\omega_{pp}^2}{\omega^2} - \frac{\omega_{pb}^2}{(\omega - kv_b)^2} \equiv \varepsilon_p(\omega) - \frac{\omega_{pb}^2}{(\omega - kv_b)^2} \qquad (22)$$

Let $f \equiv (kv_b/\omega_{pp})$ and $S \equiv kv_b - \omega \ll 1$. Taylor expanding $\varepsilon_p(\omega)$ around $\omega = kv_b$, we obtain (cf. Briggs [17])

$$\varepsilon_p(\omega) = \left(\varepsilon_p\right)_{\omega=kv_b} + S\left(\frac{\partial \varepsilon_p}{\partial \omega}\right)_{\omega=kv_b} + \mathcal{O}(S^2) = \left(1 - \frac{1}{f^2}\right) + \frac{2S}{f^3 \omega_{pp}} + \mathcal{O}(S^2)$$

Also, by Eq. (22)

$$\varepsilon_p(\omega) = \frac{\omega_{pb}^2}{S^2}$$

Hence

$$R = \frac{\omega_{pb}^2}{\omega_{pp}^2} = \left(1 - \frac{1}{f^2}\right) \frac{S^2}{\omega_{pp}^2} + \frac{2}{f^3} \frac{S^3}{\omega_{pp}^3} + \mathcal{O}(S^4)$$

or

$$R \approx -\frac{2}{f^3} \chi^3 + \left(1 - \frac{1}{f^2}\right) \chi^2 \qquad (23)$$

where

$$\chi \equiv \frac{-S}{\omega_{pp}}$$

When higher accuracy is necessary, the original quartic equation, Eq. (22) may be solved directly. Since S is a small parameter, we take Eq. (23) as our first approximation to the beam-plasma dispersion relation. Further we obtain

$$\text{Im}\ (\chi) = \omega_{imag}/\omega_{pp} \equiv \gamma/\omega_{pp} \qquad (24)$$

$$\text{Re}\ (\chi) = \frac{kv_b}{\omega_{pp}} - \frac{\omega_r}{\omega_{pp}} = f - \frac{\omega_r}{\omega_{pp}} \qquad (25)$$

$$\eta = \frac{2\Delta v}{v_b} = \frac{2\ \text{Re}\ (\chi)}{f} \qquad (26)$$

The numerical solutions of Eqs. (23-26) are plotted in Fig. 7. The saturation level [cf. Fig. 7(c)] increases monotonically even past the maximum growth rate point $kv_b/\omega_{pp} = 1.0$. This is readily justified by the fact that the saturation level is directly proportional to the velocity slip [cf. Eq. (20)], namely, the difference between the phase velocity of the growing mode and the beam velocity [cf. Fig. 7(a)].

(b) Verification by Simulations

(i) Particle Simulation (ES1)

The input parameters that we used are quite modest

$$n_b = 256 \quad , \quad n_p = 128$$

$$\omega_{pp}\Delta t = 0.2 \quad , \quad \omega_{pb}\Delta t \approx 6.3 \times 10^{-3}$$

$$NG \equiv \frac{L}{\Delta x} = 32$$

$$\frac{\tau_p}{\tau_t} \lesssim 1 \quad \left(\tau_p = \frac{2\pi}{\omega_{pp}} \quad , \quad \tau_t = \frac{L}{v_b}\right)$$

Both momentum conserving and energy conserving schemes are used as the charge and force weighting schemes. The excitation of modes is through density (i.e., position) perturbation. All wave numbers are excited initially with comparable amplitudes. The range from the starting wave energy to the saturation level is about 10^6 to 10^8.

The results in Fig. 7 show very good agreement with those of our approximation formulas, Eqs. (23)-(26). Saturation levels for all

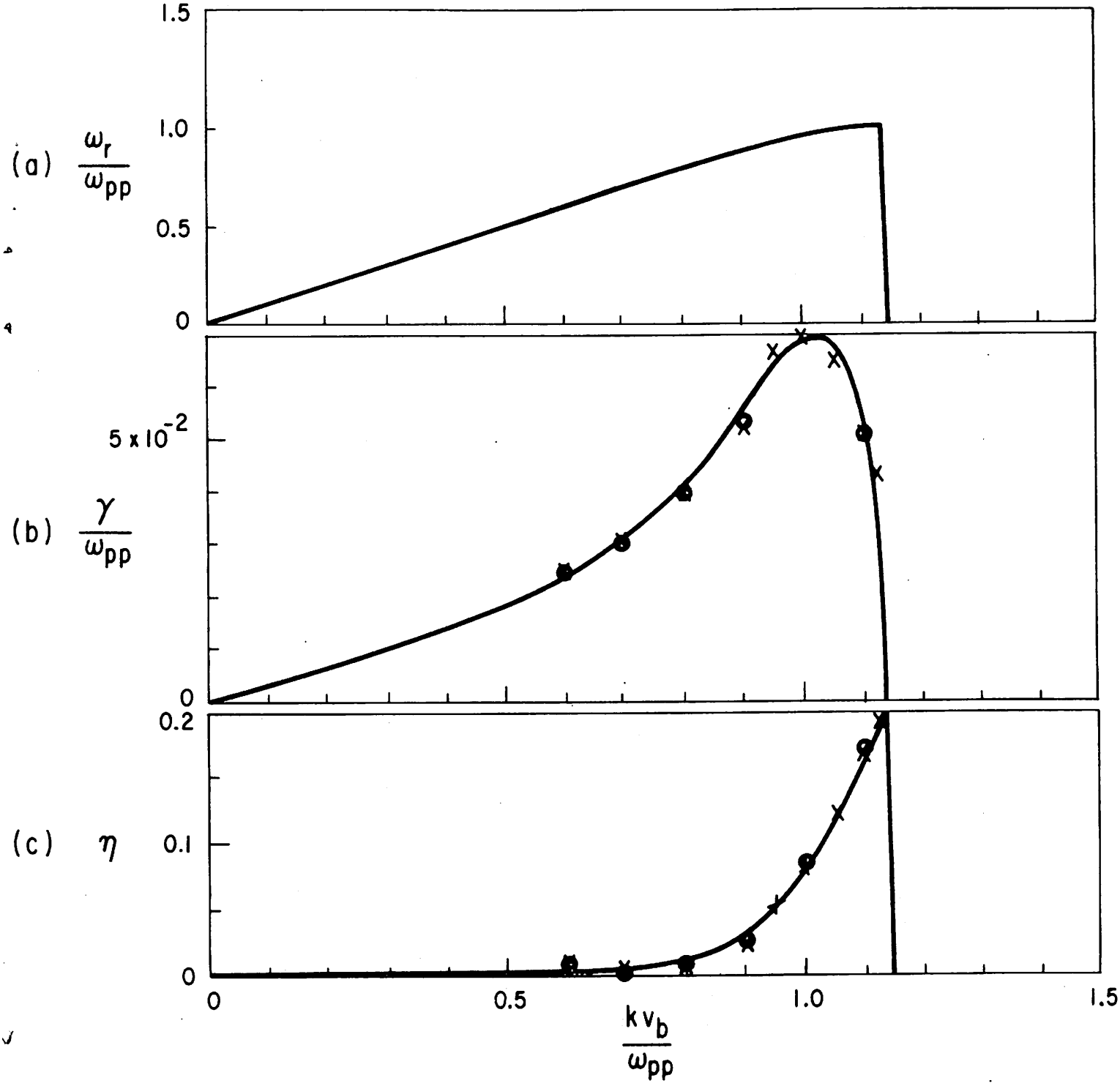

Fig. 7 Beam-plasma instability for R = 0.001: (a) real frequencies of growing modes (purely real frequencies are not plotted), (b) growth rates, and (c) saturation levels. Curves are the theoretical predictions of Eqs. (23) - (26). Single mode simulation results are marked 0 (particle code) and x (hybrid code); real frequencies (a) also agree well with the theory (not shown).

of the runs in which the most unstable mode may exist compare roughly with that calculated for the most unstable mode.

(ii) Hybrid Simulation (ES1 + EFL)

The input parameters for these cases are the same as in the corresponding particle simulations.

Since this code uses linearized Eulerian fluid equations for the plasma component, the results are expected to be good when the linearity assumption holds, that is, when the ratio of the perturbed plasma velocity to the wave phase velocity is small compared to the unity [cf. Eq. (18)]. This was verified for most of the hybrid runs, for example, $(kv_1/\omega)_{max}$ was 0.57×10^{-2} for $k_{min}(v_b/\omega_{pp}) = 0.7$, and 1.9×10^{-2} for $k_{min}(v_b/\omega_{pp}) = 1.05$ (the linear assumption holds better for the former case).

Unlike the particle code, the hybrid simulation does not generate the nonlinear harmonics of unstable modes as waves grow in time; thus the number of modes initially excited yielded important differences. As an example, for $k_{min}(v_b/\omega_{pp}) = 0.7$, we obtained $\gamma/\omega_{pp} = 2.7 \times 10^{-2}$, $\eta = 2.2 \times 10^{-3}$ when only the fundamental mode was initially excited by a sinusoidal density modulation. This should be compared with that $\gamma/\omega_{pp} = 3.1 \times 10^{-2}$, $\eta = 7.1 \times 10^{-3}$ (about three times larger) for $k_{min}(v_b/\omega_{pp}) = 0.7$ when all the modes are initially excited with comparable amplitudes (only the latter cases, i.e., all-modes-excitation, are plotted in Fig. 7).

The amplitude of the initial mode energy is also an important factor for the study of the wave saturation. This level should be quite low, as in laboratory experiments; otherwise, the simulation

saturation levels will be appreciably affected. This effect was observed in many of our runs listed here, and in ring-plasma simulations discussed in previous sections, and in relativistic beam-plasma simulations [18].

V. CONCLUSION

Hybrid codes are constructed combining an existing particle code with a linearized fluid code. The application of these codes to beam-plasm-type instabilities was presented. For the velocity space ring-plasma instability, hybrid simulations yield much better agreement with theory than do particle simulations. For the more familiar beam-plasma instability, in the absence of a magnetic field, hybrid simulations produce almost identical results to particle simulations (both of which agree with linear and nonlinear analyses), but with much reduced computing cost and noise level.

With the verification by simulations, it is shown that the saturation level is very strongly influenced by the discrete wave number spectrum, sometimes giving an order of magnitude different results by choosing slightly different off-peak (in growth rate curve) parameters, which must be considered in most simulations (whether hybrid or particle, whether magnetized or unmagnetized).

ACKNOWLEDGMENTS

The authors want to express gratitude to A. B. Langdon and W. M. Nevins for their useful suggestions and discussions.

This work was supported by the U.S. Department of Energy Contract EY-76-S-03-0034-PA128.

REFERENCES

1. C. K. Birdsall, M. J. Gerver, and N. Maron, "Ring-Plasma Instability: Theory and Simulation", Bull. Am. Phys. Soc. 21, 1148 (1976).
2. A. B. Langdon, private communication.
3. T. M. O'Neil, J. H. Winfrey, and J. H. Malmberg, "Nonlinear Interaction of a Small Cold Beam and a Plasma", Phys. Fluids, 14, 1204 (1971).
4. C. K. Birdsall and A. B. Langdon, "Plasma Physics via Computer Simulation" (to be published).
5. D. Potter, "Computational Physics", Section 9.1, John Wiley & Sons, 1973.
6. B. M. Marder, "GAP, a PIC Type Fluid Code", Mathematics of Computation 29, 434 (1975).
7. D. V. Anderson, "Collisionless Plasma Fluid Model Truncated by Tracer Particles", Proceedings of Seventh Conference on Numerical Simulation of Plasmas, June (1975).
8. J. K. Lee and C. K. Birdsall, "Particle-Fluid Hybrid Simulations Applied to Beam-Plasma and Ring-Plasma Instabilities", Proceedings of Eighth Conference on Numerical Simulation of Plasmas, PC-10, June (1978).
9. A. B. Langdon, "Investigations of a Sheet Model for a Bounded Plasma with Magnetic Field and Radiation", Ph.D. thesis, Princeton University (1970); B. I. Cohen, M. A. Mostrom, D. R. Nicholson, A. N. Kaufman, and C. E. Max, "Simulation of Laser Beat Heating of a Plasma", Phys. Fluids 18, 470 (1975).
10. S. Seiler, M. Yamada, and H. Ikezi, "Lower-Hybrid Instability Driven by a Spiraling Ion Beam", Phys. Rev. Lett. 37, 700 (1976); S. Seiler,

"Linear and Nonlinear Development of a Lower-Hybrid Wave Driven by a Perpendicular Ion Beam", Ph.D. thesis, Princeton University (1977).

11. M. Yamada and S. W. Seiler, "Anomalous Slowing of a Perpendicularly Injected Ion Beam in Both Quasilinear and Trapping Regimes", Phys. Rev. Lett. 39, 808 (1977).

12. H. Böhmer, "Excitation of Ion Cyclotron Harmonic Waves with an Ion Beam of High Perpendicular Energy", Phys. Fluids 19, 1371 (1976).

13. J. A. Tataronis and F. W. Crawford, "Cyclotron Harmonic Wave Propagation and Instabilities", J. Plasma Phys. 4, 231 (1970).

14. H. E. Mynick, M. J. Gerver, and C. K. Birdsall, "Stability Regions and Growth Rates for a Two-Ion Component Plasma, Unmagnetized", Phys. Fluids 20, 606 (1977).

15. J. K. Lee and C. K. Birdsall, "Ring-Plasma Instability; Linear Theory, Simulation, Nonlinear Behavior", Bull. Am. Phys. Soc. 22, 1109 (1977); "Velocity Space Ring-Plasma Instability, Magnetized: Parts I and II", Phys. Fluids 22 (1979), (to be published).

16. W. E. Drummond, J. H. Malmberg, T. M. O'Neil, and J. R. Thompson, "Nonlinear Development of the Beam-Plasma Instability", Phys. Fluids 13, 2422 (1970).

17. R. J. Briggs, "Two-Stream Instabilities", in "Advances in Plasma Physics", vol. 4, pp. 43-77, John Wiley & Sons, 1971.

18. L. E. Thode and R. N. Sudan, "Plasma Heating by Relativistic Electron Beams", Phys. Fluids 18, 1558 (1975).